LEAST SQUARES MULTIPLE IMAGES MATCHING FOR LARGE COVERAGE AERIAL IMAGE AND SMALL COVERAGE UAV IMAGE

Kai-Zhi Zhan[a], Tee-Ann Teo[b]

[a] Master degree student, Dept. of Civil Engineering, National Chiao Tung University, Hsinchu, Taiwan 30010.

[b] Associate Professor, Dept. of Civil Engineering, National Chiao Tung University, Hsinchu, Taiwan 30010.

E-mail: claus6310@yahoo.com.tw; tateo@mail.nctu.edu.tw

KEYWORDS: Multi-view image, least squares matching, geometric constraint.

ABSTRACT

Unmanned aerial vehicle (UAV) is widely used to acquire high resolution imagery at multiple viewing angles. The benefit of multi-view images is to provide better intersection geometry. To compare the UAV and traditional aerial photogrammetry, UAV derives 3D structure from different view angles but traditional aerial photogrammetry usually takes photo at vertical view. The integration of these two platforms may improve the viewing geometry. However, there are some difficulties to integrate two platform images as different image-scales, occlusions, illumination changes and acquisition geometry. In this study, we propose a robust image matching method based on least squares matching. The multi-view least squares matching (MVLSM) combines multi-view geometry and least squares matching method to determine the conjugate points. The initial tie points and images scale are obtained manually. Then, we use the MVLSM in precise matching .The test images are UltraCam aerial image and sensefly eBee UAV images. The test area is located at National Chiao Tung University, Taiwan. The MVLSM may improve the matching accuracy at sub-pixels level. Moreover, integrating aerial photo and UAV images matching strategy will be beneficial to the data fusion, data analysis and other applications.

1. INTRODUCTION

1.1 Motivation

Unmanned aerial vehicle (UAV) which has integrated Global Navigation Satellite System, (GNSS), Inertial Navigation System (INS), consumer camera, and flying controller is commonly used to produce maps at small coverage. It can acquire high resolution and high overlap rate aerial images at multiple viewing angles agilely. Employing Direct Geo-referencing technology can provide initial position and exterior orientation of exposure center. To compare the UAV and traditional aerial photogrammetry, the cost of UAV imagery is much cheaper than traditional aerial photogrammetry. Besides, UAV flies in a close flying height and takes images at different view angles despite of higher and vertical viewing geometry of traditional aerial imagery. However, traditional aerial photogrammetry usually equipped with metric cameras and stable platforms which can provide superior parameters of exposure center. Hence, integration of these two platforms may improve the viewing geometry and the positioning accuracy. Figure 1 gives the illustration of improving intersection geometry via image integration.

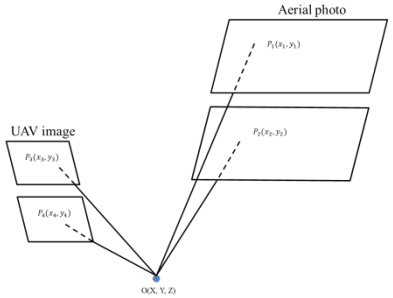

Figure 1 Improving intersection geometry via integration of UAV and aerial photo

1.2 Related study

Image matching is an important step to integrate difference images data. Image matching algorithms can be classified into area-based and feature-based. The area-based algorithms are based on the images intensity in

correlation metrics, the feature-based algorithms are finding correspondence between image features such as points, lines, and contours (Gruen, 2012). Traditionally, pairwise image matching only considered the correlation between two images. Multi-image matching algorithms which consider overall images were proposed to improve the geometrical consistency. The multi-image matching algorithms can be classified into sequential image matching and multiple image matching. The sequential image matching confirmed the location of conjugate points in image pairs sequentially. On the other hand, multiple images matching considering the spatial relations of conjugate points in all images can provide redundancy. Therefore, multiple images matching are more favorable for the purpose of space intersection.

Many studies discuss about multiple images matching. Zhang and Gruen (2006) proposed a multiple images matching called Geometrically Constrained Cross Correlation method (GCCC) to derive digital surface model (DSM). In their study, they calculated the Sum of Normalized Cross Correlation (SNCC) between target images and search images, estimated the correct matching position. Vertical Line Locus (VLL) and Modified Vertical Line Locus (MVLL) were applied in multi-images to produce DSM. The concept of the method is to fix a plane coordinate (x,y), and to give some estimated elevation for calculating the correlation of images (Noh et al, 2012, Ji et al, 2012). Least-square matching (LSM) is a robust image matching algorithms (Ackermann, 1984, Gruen, 1985). The main concept of LSM is to minimize the difference of the gray value. The advantage of LSM is its sub-pixel level matching and accuracy assessment. Gruen and Baltsavias (1986) developed a multi-image LSM approaches which combined the LSM, epipolar geometric constraint and collinearity condition. Elaksher (2008) applied the multi-image LSM in refinement the urban area digital elevation models (DEM). Baltsavias (1991) discussed multi-image geometric constraint matching. Yang et al (2012) presented a multistage matching which integrate Scale-Invariant Feature Transformation (SIFT), multi-image LSM and NCC to solve the false matching for oblique images.

Most of the studies focused on image matching for only one platform images. Few studies discussed the multi-view matching of UAV images and aerial photo. If one can develop the multi-view matching approach for UAV images and aerial photo, it might be beneficial to the data fusion, data analysis and other applications.

1.3 Purpose

The objective of this study is to integrate UAV images and aerial photo. For the purpose, we apply multi-view least squares matching (MVLSM) which combines multi-view geometry and least squares matching method for the determination of precise conjugate points. In general, the difficulties to integrate UAV images and aerial photo derives from these two platforms have different image-scales, occlusions, illumination changes and acquisition geometry. Besides, UAV is light weight and short wing. So crosswind may cause image blur and large variety of exterior orientation. The major work includes three major steps: data preprocessing, bundle adjustment, and precise matching. Due to the large lens distortion of consumer cameras in UAV, data preprocessing is to remove this distortion. In bundle adjustment, we select tie points from obviously ground feature, e.g. road mark, to recover the exterior orientation. The location and the calculated images scale of tie points are obtained as the initial value in next step. Finally, the MVLSM for UAV images and aerial photo is used to refine the tie points. Before matching, we projected images from image space to object space to overcome problem of image-scales and occlusions. The illumination changes can be reduced by applied gray value normalization.

2. METHODOLOGY

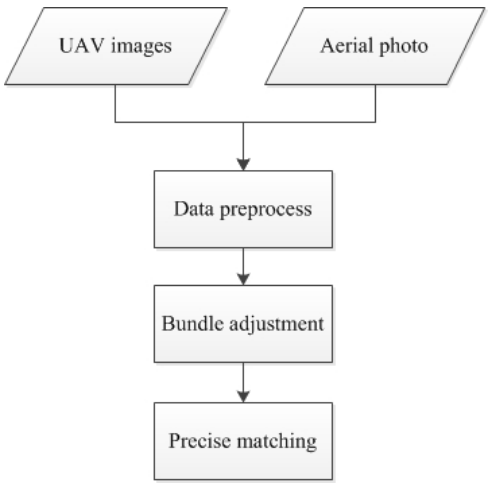

Figure 2 The workflow of the proposed method

Figure 1 shows the research workflow. The first step is data preprocess. UAV images have some distortion, blur interior orientation unstable problems. In data preprocessing, we corrected the lens distortion. The second step is bundle adjustment, recovered the accurate exterior orientation, at the same time, obtain initial tie points and images scale. The final step is precise matching. The multi view least square matching is used to refine tie points and obtain the sub-pixel accuracy matching results.

2.1 Data preprocessing

Because UAV is light weight and short wing, images would blur and exterior would orientation unstable when taking photo with the crosswind. In addition, the interior orientation of consumer camera is more unstable than frame camera, and the distortion is more serious than large frame camera too. In the research, we remove most of distortion and produce undistorted images. Then, we applied the undistorted images and initial orientation in the next step.

2.2 Bundle adjustment

Since precise matching needs good initial value, we used the bundle adjustment to recover accurate exterior orientation. Besides, we select significant feature points on ground as tie point. Moreover, we calculated the initial parameters for LSM. In order to transform the image coordinate to world coordinate, DGPS surveying is used to obtain the ground control points (GCP) and determine the ground coordinates.

2.3 Precise matching

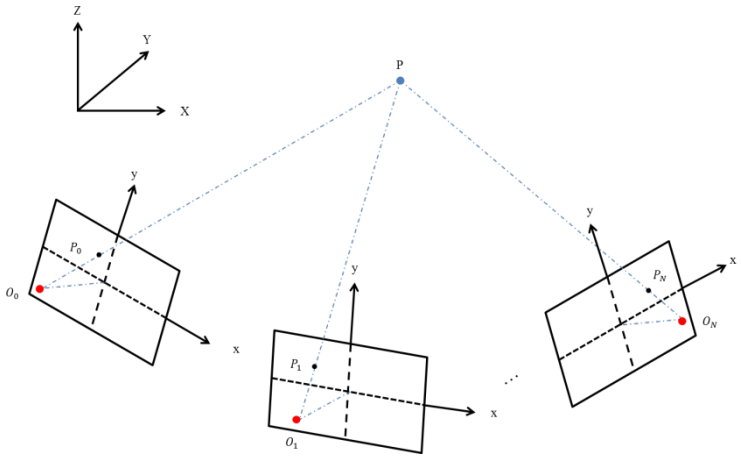

Figure 3 Multiple images arrangement for point (Gruen and Baltsavias, 1986)

The multiple images precise matching is based on LSM. Multiple images arrangement for point is shown Figure 3. The main concept of the LSM is minimization of the difference of gray value between images. The v_g is the gray value difference, the $g_t(x,y)$ is gray value of target image at coordinate (x,y), and the $g_s(x',y')$ is gray value of of search image at image coordinate(x',y').

$$\sum {v_g}^2 \rightarrow min \quad (1)$$

$$v_g = g_s(x',y') - g_t(x,y) \quad (2)$$

We added small displacement at x, y direction for description the location of minimum gray value difference. So the equation (2) is transform to equation (3). .

$$v_g = g_s(x+dx,y+dy) - g_t(x,y) \quad (3)$$

Because the equation (3) is nonlinear, it is linearized to (4)

$$v_g = g_s(x,y) - g_t(x,y) + g_x dx + g_y dy \quad (4)$$

$$g_x = \frac{\partial g_s(x,y)}{\partial x}$$

$$g_y = \frac{\partial g_s(x,y)}{\partial y} \quad (5)$$

g_x, g_y are the gradient of gray value at x and y direction.

Using the notations

$$\mathrm{X}^T = [dx \quad dy] \quad (7)$$

$$l = g_s(x,y) - g_t(x,y) \quad (8)$$

$$\mathrm{A} = [g_x \quad g_y] \quad (9)$$

Where X^T = the unknown parameter vector, l is the observation vector and A is design matrix.

Solve the unknown parameter

$$V = AX - L \tag{10}$$

$$\mathrm{X} = (A^T P_A A)^{-1}(A^T P_A L) \tag{11}$$

P is the weight matrix. In the study, we assume it is equal weight.

The conjugate points in the image must follow the collinear equation, the equation (12).

$$x - x_p = -f\frac{m_{11}(X-X^c)+m_{12}(Y-Y^c)+m_{13}(Z-Z^c)}{m_{31}(X-X^c)+m_{32}(Y-Y^c)+m_{33}(Z-Z^c)} = F(X,Y,Z)$$

$$y - y_p = -f\frac{m_{21}(X-X^c)+m_{22}(Y-Y^c)+m_{23}(Z-Z^c)}{m_{31}(X-X^c)+m_{32}(Y-Y^c)+m_{33}(Z-Z^c)} = G(X,Y,Z) \tag{12}$$

(x_p, y_p) is the principal point, f is focal length, $m_{11}\sim m_{33}$ is rotation matrix of image, (X^c, Y^c, Z^c) is the camera position, (X, Y, Z) is the object coordinate of point, (x, y) is the image coordinates of point.

Linearization of equations (12)

$$dx + \frac{\partial F}{\partial X}dX + \frac{\partial F}{\partial Y}dY + \frac{\partial F}{\partial Z}dZ + F_0 + x - x_p = 0$$

$$dy + \frac{\partial G}{\partial X}dX + \frac{\partial G}{\partial Y}dY + \frac{\partial G}{\partial Z}dZ + G_0 + \mathrm{y} - y_p = 0 \tag{13}$$

Using the notations

$$\mathrm{Y}^T = [dx \quad dy \quad dX \quad dY \quad dZ] \tag{14}$$

$$K^T = [F_0 + x - x_p \quad G_0 + \mathrm{y} - y_p] \tag{15}$$

$$\mathrm{B} = \begin{bmatrix} 1 & 0 & \frac{\partial F}{\partial X} & \frac{\partial F}{\partial Y} & \frac{\partial F}{\partial Z} \\ 0 & 1 & \frac{\partial G}{\partial X} & \frac{\partial G}{\partial Y} & \frac{\partial G}{\partial Z} \end{bmatrix} \tag{16}$$

Solve the unknown parameter

$$V_c = BY - K \tag{17}$$

$$\mathrm{Y} = (B^T P_B B)^{-1}(B^T P_B K) \tag{18}$$

Equations (10) and (17) are connected via the shift parameter dx, dy that appears in both equations, and form the joint system.

$$\begin{cases} V = AX - L \\ V_c = BY - K \end{cases} \tag{19}$$

Furthermore, the solution became equation (20)

$$\widehat{\mathrm{X}} = (A^T P_A A + B^T P_B B)^{-1}(A^T P_A L + B^T P_B K) \tag{20}$$

2.4 Accuracy assessment

The accuracy assessment is based on the least square theory. The joint system accuracy

$$\sigma_0{}^2 = \frac{V^T P_A V + V_c{}^T P_B V_c}{r} \tag{21}$$

$\mathrm{r} = n - u$, redundancy, n = number of observations u = number of parameters.

3. EXPERIMENTAL

3.1 Experimental Data

The Test area is located at National Chiao Tung University, Hsinchu city, Taiwan. The aerial photo is acquired by UltraCam-D and the UAV images is obtained by SenseFly eBee UAV. The test images are shown in figures 3(a) to (h). Figures 3(a) to 3(d) are UltraCam aerial photo, while figures 3(e) to 3(h) are UAV images. In addition, the ground coverage of images is shown as Figure 4. The small triangle represents GCP distribution in the images, and the small square represents tie points distribution in the images. The flying height of UAV and UltraCam are about 300m and 2000m. Table1 summarizes the related parameters for the images. Nine GCPs were measured by differential-GPS, used Trimble NetR9 GNSS reference receiver.

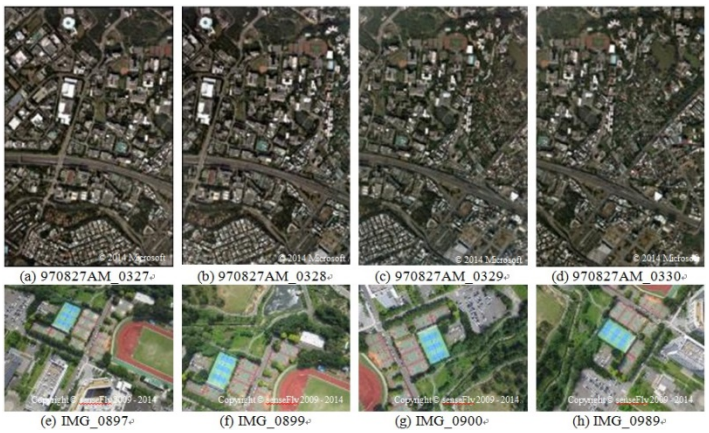

Figure 3 Test data

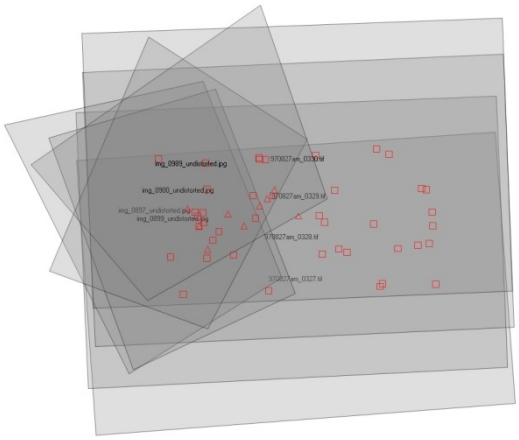

Figure 4 Footprint of test data

Table 1 information related to test images

Sensor	Canon IXUS125	UltraCam-D
Image size	4608 x 3456	7500 x 11500
Acquisition year	2013	2006
Focal length (mm)	4.43	101.40
GSD (m)	0.06	0.20
Flying height	300	2000

3.2 Experimental items

The validation experiments are divided into three parts: data preprocessing, bundle adjustment accuracy and precise matching accuracy assessment.

3.3 Data preprocessing

In data preprocess, we used the interior orientation parameters to produce undistorted UAV images. The undistorted images were generated by eBee Postflight. It removed almost lens distortion which caused by unstable systems.

3.4 Bundle adjustment accuracy

The bundle adjustment was implemented in ERDAS LPS. We compared the accuracy of only UAV images and UAV images join with UltraCam photo before precise matching. The only UAV image block contained 4 full control points and 16 tie points in bundle adjustment. Moreover, the UAV join with UltraCam photo block added 5 full control points and 36 tie points in bundle adjustment. The results of bundle adjustment show as Tables 2 and 3. The table 2 and 3 show that integration of UAV and aerial photos can improve the intersection geometry actually.

Table 2. only UAV images bundle adjustment accuracy (4 images)

Total image unit-weight RMSE(pixels)		0.636	
Control point ground XRMSE(m)	0.000	Check point ground XRMSE(m)	0.102
Control point ground YRMSE(m)	0.000	Check point ground YRMSE(m)	0.094
Control point ground ZRMSE(m)	0.000	Check point ground ZRMSE(m)	1.933
Control point image XRMSE (pixels)	0.679	Check point image XRMSE (pixels)	3.819
Control point image YRMSE (pixels)	0.674	Check point image YRMSE (pixels)	4.865

Table 3. UAV images join UltraCam photo bundle adjustment accuracy (8 images)

Total image unit-weight RMSE(pixels)		0.500	
Control point ground XRMSE(m)	0.000	Check point ground XRMSE(m)	0.051
Control point ground YRMSE(m)	0.000	Check point ground YRMSE(m)	0.135
Control point ground ZRMSE(m)	0.000	Check point ground ZRMSE(m)	0.164
Control point image XRMSE (pixels)	0.462	Check point image XRMSE (pixels)	0.306
Control point image YRMSE (pixels)	0.419	Check point image YRMSE (pixels)	0.213

3.5 Precise matching accuracy assessment

In this study, we selected 15 points to assess refined point accuracy. The refined points were obtained by the proposed MLSM. These refined point coordinates were input data, and we used bundle adjustment for assessment. The bundle adjustment of refined points is shown as Table 4. To compare the Tables 3 and 4, the results show that using MLSM can improve accuracy of the tie point. Figure 5 is shown as the image location of control point before (red cross) and after (green cross) MLSM.

Table 4 refined points bundle adjustment accuracy

Total image uint-weight RMSE(pixels)		0.426	
Control point ground XRMSE(m)	0.000	Check point ground XRMSE(m)	0.051
Control point ground YRMSE(m)	0.000	Check point ground YRMSE(m)	0.135
Control point ground ZRMSE(m)	0.000	Check point ground ZRMSE(m)	0.164
Control point image XRMSE (pixels)	0.462	Check point image XRMSE (pixels)	0.306
Control point image YRMSE (pixels)	0.419	Check point image YRMSE (pixels)	0.213

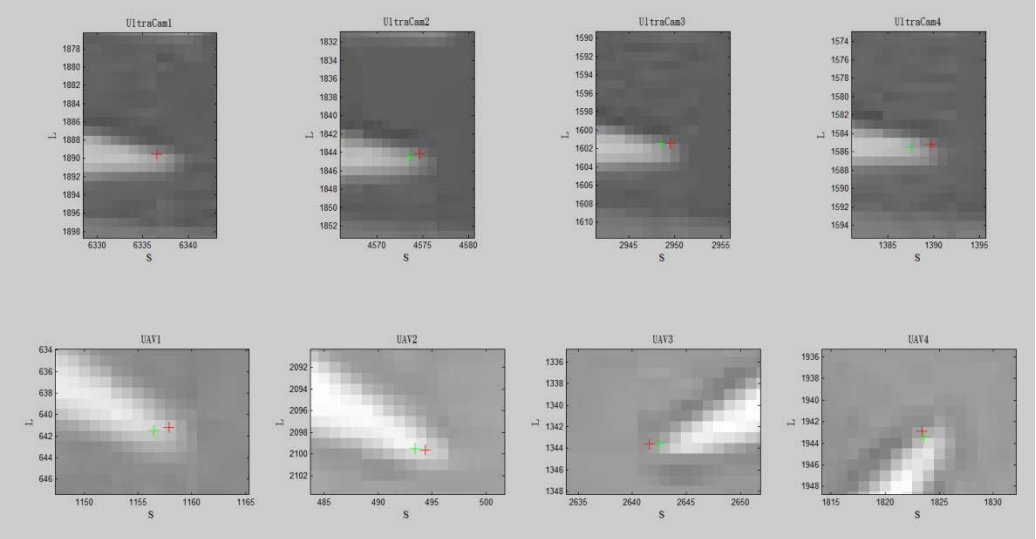

Figure 5 the matching result

3.6 Pairwise and multiple-image LSM

In addition, we also compared with pairwise least square matching (PLSM). The pairwise matching did not consider all the radiometric and geometric constrains simultaneously. We used the PLSM to refine 15 points (same as section 3.5). The matching results were used in bundle adjustment for assessment. Table 5 show the results. To compare the Tables 4 and 5, the precision of MLSM was better than PLSM

Table 5 pairwise LSM refined points bundle adjustment accuracy

Total image uint-weight RMSE(pixels)		0.8329	
Control point ground XRMSE(m)	0.000	Check point ground XRMSE(m)	0.051
Control point ground YRMSE(m)	0.000	Check point ground YRMSE(m)	0.135
Control point ground ZRMSE(m)	0.000	Check point ground ZRMSE(m)	0.164
Control point image XRMSE (pixels)	0.462	Check point image XRMSE (pixels)	0.306
Control point image YRMSE (pixels)	0.419	Check point image YRMSE (pixels)	0.213

4. CONCLUSIONS

In this study, we presented a multiple images matching based on least square adjustment. The multi-view least squares matching consider both radiometric and geometric constrains for multiview images. The proposed scheme integrated the UAV images and UltraCam aerial photo for improving better intersection geometry. In order to solve the UAV interior and exterior orientation unstable problem, we produced the undistorted images. To compare UAV only and UAV+UltraCam, the geometrical accuracy has improving. Besides, we also compared MLSM and pairwise LSM. The result shows that after refine points, the MLSM has better performance than pairwise LSM.

The future works include: (1) In the Bundle adjustment, tie points was select manually. In the future, we will use automatic registration algorithms to obtain well accuracy tie points. (2) In the precise matching, we used a simple adjustment model. In the future, we will expand the adjustment model to get more precise coordinates. (3) In the precise matching, we assume weight for every observation. In the future we will consider different conditions to give different weights for observations.

ACKNOWLEDGMENT
The authors would like to thank the Control-Signal Co., Ltd in Taiwan for providing the test data sets.

REFERENCE

1. Ackermann, F. 1984. Digital image correlation: Performance and potential application in photogrammetry. Photogrammetric Record 11 (64):429-439.
2. Baltsavias, E.P., 1991. Multiphoto geometrically constrained matching. PhD Dissertation, Report No. 49, Institute of Geodesy and Photogrammetry, ETH Zurich, Switzerland.
3. Elaksher, A., 2008. A multi-photo least squares matching algorithm for urban area DEM refinement using breaklines, The International Archives of the Photogrammetry, Remote Sensing and Spatial Information Sciences, 37(B3a): 33-38.
4. Gruen, A., 1985. Adaptive least squares correlation: a powerful image matching technique. South African Journal of Photogrammetry, Remote Sensing and Cartography 14 (3): 175–187.
5. Gruen, A., 2012. Development and status of image matching in photogrammetry, The Photogrammetric Record, 27(137): 36-57.
6. Gruen, A., and Baltsavias, E.P., 1986. Adaptive least squares correlation with geometrical constraints, International Society for Optics and Photonics, International Technical Symposium, Europe, pp. 72-82.
7. Ji, S., Zhang, Y. S., Fan, D. Z., and Dai, C. G., 2012. Integration of multi-view matching models for linear array digital imagery, In Automatic Control and Artificial Intelligence (ACAI 2012), International Conference on, pp. 1244-1247.
8. Noh, M. J., Cho, W., and Bang, K. I., 2012. Highly Dense 3D Surface Generation Using Multi-image Matching. ETRI Journal, 34(1): 87-97.
9. Yang, H., Zhang, S., and Wang, Y., 2012. Robust and precise registration of oblique images based on scale-invariant feature transformation algorithm. Geoscience and Remote Sensing Letters, IEEE, *9*(4): 783-787.
10. Zhang L., and Gruen, A., 2006. Multi-image matching for DSM generation from IKONOS imagery, ISPRS Journal of Photogrammetry & Remote Sensing, 60: 195–211.